Modeling Study of the Sorption-Enhanced Reaction Process for CO2 Capture. I.

Model Development and Validation

H.T.J. Reijers

J. Boon

G.J. Elzinga

P.D. Cobden

W.G. Haije

R.W. van den Brink

Published in the Ind. Eng. Chem. Res., 2009, 48 (15) pp 6966-6974

ECN-W--09-040 December 2009

Modeling Study of the Sorption-Enhanced Reaction Process for CO_2 Capture. I. Model Development and Validation

Hendricus Th. J. Reijers,* Jurriaan Boon, Gerard D. Elzinga, Paul D. Cobden, Wim G. Haije, and Ruud W. van den Brink

Hydrogen & Clean Fossil Fuels, Energy research Centre of The Netherlands, P.O. Box 1, 1755 ZG, Petten, Netherlands

A one-dimensional reactor model has been developed to describe the performance of a sorption-enhanced steam-methane reforming and water−gas shift reactor. In part I of this paper, the model is verified using the analytical solution for the breakthrough curve and validated using the results of laboratory-scale CO_2 sorption-only experiments. Langmuir and Freundlich isotherms are fitted to an experimentally derived adsorption isotherm, while a linear driving force model is used to describe the sorption kinetics. The breakthrough profile is accurately described using the Freundlich isotherm. This holds also when the purge flow or duration of the desorption step are decreased, provided the mass transfer coefficient is changed accordingly during the desorption step. A sensitivity analysis shows that the breakthrough profile is sensitive to the adopted isotherm model and its parameters. The molecular diffusion coefficient affects the slope of the breakthrough curve, while particle size and heat of adsorption show hardly any effect. In part II, the model will be applied to laboratory-scale sorption-enhanced steam-methane reforming experiments.

Introduction

The sorption-enhanced reaction process (SERP) offers an attractive possibility for precombustion CO_2 capture.[1] Hydrogen production and CO_2 capture are combined in one step, resulting in lower capital costs. The hydrogen is produced in the reformer according to the steam-methane reforming (SMR) reaction

$$CH_4 + H_2O \leftrightarrow CO + 3H_2 \qquad (\Delta H^\circ_{298} = +206 \text{ kJ/mol}) \tag{1}$$

and the water−gas shift (WGS) reaction

$$CO + H_2O \leftrightarrow CO_2 + H_2 \qquad (\Delta H^\circ_{298} = -41 \text{ kJ/mol}) \tag{2}$$

A suitable sorbent is mixed with the SMR catalyst. The CO_2 produced is selectively removed by the sorbent. Thus, the reaction equilibria shift to the product side, enabling the SMR and WGS reactions and the CO_2 capture processes to be combined in one single step. The same CH_4 conversion may be obtained at much lower temperatures, say between 723 and 823 K, than in conventional SMR without sorbent, which is performed typically between 1123 and 1223 K. The sorbent must be able to capture CO_2 at relatively high temperatures. Compounds like amine solutions, physical solvents (e.g., Selexol), active carbons, and zeolites remove CO_2 at temperatures below 373 K and cannot be used at higher temperatures. Suitable sorbents include metal oxides, hydrotalcites, lithium metal oxides, and double salts.[1] Alternatively, the sorbent may be mixed with a WGS catalyst in a separate reactor downstream of the steam-methane reformer, enabling all reactions except for the SMR reaction to be combined in one reactor.[2] The advantage of the second option compared with the first one is that it is much easier to drive the WGS reaction to completion by SERP than the SMR reaction. The latter requires the sorbent to be capable to adsorb down to very low CO_2 concentrations to obtain an acceptable CH_4 conversion.[3] The CO_2 concentration should be reduced to 270 ppm at 1 bar, and to 10 ppb at 17 bar to obtain a CH_4 conversion of 90% at 673 K.

Any system using SERP should include a regeneration step to remove the adsorbed CO_2 since the sorbent is saturated after some time with CO_2. Thus, a batch process is needed in which the reactor is periodically subject to a series of steps at different conditions for the desired processes: sorption-enhanced reaction, depressurization, steam purge, and repressurization.[4]

The research by Air Products in the 1990s showed that hydrotalcite (HTC) worked satisfactorily as CO_2 adsorbent in the temperature range 673−773 K.[4,5] The CO_2 sorption was strongly enhanced by impregnating or promoting HTC with K_2CO_3, denoted as kHTC. In a previous paper, results of laboratory-scale experiments (flows between 30 and 100 mL/min, sample weight of 3 g) have been reported using this material.[1] Commercial HTCs were used (PURAL MG70, PURAL MG61 HT, PURAL MG50, and PURAL MG30) obtained from SASOL, next to in-house prepared HTCs. They were loaded with 22 wt % K_2CO_3 and adsorbed between 0.28 and 0.44 mmol CO_2/g adsorbent at 673 K and atmospheric pressure using a feed gas containing 5% CO_2, 29% H_2O, and balance N_2. A proof-of-principle test was performed demonstrating the viability of SERP for SMR. The average CH_4 conversion was 95%, much higher than the equilibrium conversion of CH_4 without adsorbent (53%). It was found that the amount of steam required for complete desorption of CO_2, expressed as the S/CO_2 ratio, the amount of steam (in moles) per mole desorbed CO_2, is too large. This ratio is an important parameter for the determination of the system efficiency since steam production is very energy-intensive.[3] Complete desorption is usually not required. There is a trade-off between the actual working capacity of the adsorbent bed and the S/CO_2 ratio. Efficiencies were calculated for some precombustion SERP-based systems for electricity production with CO_2 capture, using natural gas as fuel and promoted HTC as adsorbent. Assumptions were made on the CH_4 conversion and carbon recovery. It was shown that for an acceptable system efficiency, the required total amount of steam (in moles) for both SMR and CO_2 purge,

* To whom correspondence should be addressed. Tel.: +31 (0) 224-564588. Fax: +31 (0) 224-568489. E-mail address: reijers@ecn.nl.

10.1021/ie801319q CCC: $40.75

expressed per mole CH_4 and per mole CO_2, respectively, should not exceed 7.

To predict the performance of large-scale reactors, a reactor model is needed next to the results of dedicated small-scale experiments. A model for a fixed-bed SERP reactor has been developed which includes the SMR and WGS reactions, together with a description of the CO_2 sorption process. The purpose of this paper is to validate this model using the results of CO_2 sorption-only experiments. Ding and Alpay have compared their experimental breakthrough curves with calculated ones.[6] The experimental data show a large scatter. In the experiments shown here, an attempt is made to improve this. Special attention will be paid to the effect of the adopted model isotherm and axial dispersion. Also the effect of an incompletely desorbed bed on the calculated breakthrough and desorption profiles of CO_2 will be assessed. Besides, a sensitivity study is performed to determine the effect of several input parameters. Results of SERP laboratory-scale experiments using an adsorbent−catalyst mixture will be used for validation in part II of this series.[7]

Reactor Model

Below, the assumptions and equations used in this model are given. Other groups have used a similar model for fixed bed, SERP reactors.[8−11] In part II of this series, an overview of their work will be given.[7]

The following assumptions have been made:

- The reactor is a tubular, fixed-bed reactor, operated dynamically.
- The flow pattern can be described by an axially dispersed plug flow model.
- The model is one-dimensional. Radial gradients of the concentrations, adsorbent loading, velocity, pressure, and temperature are not taken into account.
- The steady-state approximation is used for the momentum balance equation.[12]
- The mass and heat transfer between gas and solid is sufficiently fast, making interparticle gradients of concentrations and temperature negligible.
- Heat can be supplied to the bed via the reactor wall.
- All gaseous substances are considered as ideal gases.
- The packing consists of monodisperse particles. If both adsorbent and catalyst particles are present, they form a homogeneous mixture.
- The SMR and WGS reactions are the only ones that are considered.
- An effectiveness factor of unity is used for diffusion limitation in the catalyst, as determined by Ding and Alpay using different catalyst particle size fractions.[8]
- Carbon dioxide is the only adsorbed species.
- The linear driving force (LDF) approximation is used to describe the sorption kinetics (see below).
- The Langmuir and Freundlich isotherms are the only ones used here to describe the experimental CO_2 adsorption isotherm. Although the model is used here to describe laboratory-scale experiments, the above assumptions also largely apply to an industrial reactor. In contrast to the laboratory-scale reactor reported here, the large-scale reactor is usually operated in pressure-swing mode. The reactor is pressurized during the feed step, while regeneration is performed at a much lower, usually atmospheric pressure. A blowdown and repressurization step are in between these steps, so that the process cycle includes at least four steps. For a large-scale reactor, the following additional remarks must be made:
- For steam-methane reformers, the radial temperature gradient may be neglected if the reactor tube to particle diameter ratio is less than 6 as a rule of thumb.[13] For industrial reformers, this condition is usually not fulfilled, and a two-dimensional model must be used. The radial gradient is between 10 and 40 K, depending on the reactor design, the axial position, and the catalytic activity.[14] For a SERP reactor, the net heat required may be different. On one hand, heat is produced in the reactor due to the exothermic adsorption of CO_2. On the other hand, the reactor size is increased due to the presence of adsorbent. In addition, the operation conditions (feed flow, temperature, and pressure) may be different. To check if radial gradients must be taken into account for a SERP reactor at given conditions, at first a one-dimensional model may be used. If large differences between wall and bed temperature are found to occur, a two-dimensional model may be required.
- The steady-state approximation for the momentum balance remains valid for the feed and regeneration steps where the pressures at the reactor inlet and outlet do not change. However, during pressurization and blowdown the dynamic pressure effects are much more pronounced. Nevertheless, Sereno and Rodrigues have shown that the steady-state approximation also holds for the pressurization and blowdown steps of a pressure-swing adsorption cycle.[12] To check if it is also valid for a SERP reactor, at first the equations are solved using the steady state approximation. Then, the values of the neglected terms are evaluated (see the Supporting Information). If these are negligible compared with the other terms of the momentum balance equation, the approximation holds. If not, the neglected terms must be included.
- A different effectiveness factor may be used. Xiu et al. calculated values of the effectiveness factor for a SERP reactor explicitly.[15] They found values around 0.8 for particles of 3 mm diameter, at temperatures between 723 and 763 K, and pressures between 2.2 and 8.9 bar, using Xu and Froment kinetics and Fickian intraparticle diffusion. In the work of Ochoa-Fernández et al.,[16] reference is made to calculations of intraparticle concentration gradients for catalyst particles of 5 mm diameter at 848 K, 5 atm total pressure, and typical SERP bulk gas compositions, using Xu and Froment kinetics. These result in effectiveness factors between 0.2 and 0.8. However, they also report that the model results are insensitive to variations in the effectiveness factors.
- Since the Freundlich isotherm is empirical, different parameters may be required at different operating temperature or pressure. Work by our group is in progress to come to a fundamental understanding of the CO_2 adsorption and desorption mechanism, applicable at all relevant temperatures and pressures.

The following equations are solved simultaneously:

$$\varepsilon_t \frac{\partial c_i}{\partial t} + \frac{\partial (u c_i)}{\partial z} = \varepsilon_b \frac{\partial}{\partial z}\left(D_{ax} \frac{\partial c_i}{\partial z}\right) - \rho_{b,ads} \frac{\partial q_i}{\partial t} + \rho_{b,cat} r_i \tag{3}$$

for the six components $i = CH_4$, H_2O, H_2, CO, CO_2, and N_2, where the sorbent loading with component i, q_i, is nonzero only for CO_2,

$$(\varepsilon_t c C_{v,gas} + \rho_{b,cat} C_{p,cat} + \rho_{b,ads} C_{p,ads}) \frac{\partial T}{\partial t} = \frac{\partial}{\partial z}\left(k_z \frac{\partial T}{\partial z}\right) - c C_{p,gas} u \frac{\partial T}{\partial z} - \rho_{b,ads} \Delta H_{ads,CO_2} \frac{\partial q_{CO_2}}{\partial t} + \rho_{b,cat} \sum_i H_i r_i + \frac{4U}{d_t}(T_w - T) + \varepsilon_t \frac{\partial p}{\partial t} \tag{4}$$

and

$$\frac{\partial p}{\partial z} = -K_D u - K_V u|u| \tag{5}$$

Equations 3−5 represent the material balance, energy balance and momentum balance equations, respectively. They are solved by a finite difference method using a Matlab software package together with the equation obtained by summing eq 3 over all six components:

$$\varepsilon_t \frac{\partial c}{\partial t} + \frac{\partial (uc)}{\partial z} = -\rho_{b,ads} \frac{\partial q_{CO_2}}{\partial t} + \rho_{b,cat} \sum_i r_i \tag{6}$$

where $c = \sum_i c_i$ has been used, and the relation for the linear driving force (LDF)

$$\frac{\partial q_{CO_2}}{\partial t} = k_{LDF}(q^*_{CO_2} - q_{CO_2}) \tag{7}$$

where $q^*_{CO_2}$ is the equilibrium CO_2 loading of the adsorbent, q_{CO_2} is the actual CO_2 loading averaged over the particle volume, and k_{LDF} is a lumped parameter for the sorption rate of CO_2 by the particle taking into account all mass transfer. Boundary conditions and details of the method of solution of the above equations are given in the Supporting Information.

Two model isotherms are used here: the Langmuir isotherm which can be derived straightforwardly from certain assumptions[17]

$$q^*_{CO_2} = \frac{mbp_{CO_2}}{1 + bp_{CO_2}} \tag{8}$$

and the empirical Freundlich isotherm given by

$$q^*_{CO_2} = k\left(\frac{p_{CO_2}}{101325}\right)^{1/n} \tag{9}$$

where $q^*_{CO_2}$ denotes the equilibrium loading and p_{CO_2}, expressed in Pascal, the partial CO_2 pressure. The parameters m, b, k, and n (with $n > 1$) are determined by fitting the model isotherm to the experimentally obtained one.

The Freundlich isotherm differs from the Langmuir isotherm in two aspects:

• In the limit $p_{CO_2} \to 0$, $\partial q^*_{CO_2}/\partial p_{CO_2}$ becomes infinite for the Freundlich isotherm since $n > 1$, while it shows the proper Henry's law behavior for a Langmuir isotherm.

• At high p_{CO_2}, the sorbent loading continues to increase for the Freundlich isotherm, while the Langmuir isotherm asymptotically approaches monolayer coverage.

As a consequence, the Freundlich isotherm is expected to work satisfactorily for given k and n values only in a limited CO_2 pressure and temperature range. The Langmuir model assumes the surface of the adsorbent to be homogeneous. From experimental studies on Mg−Al hydrotalcites, it has become clear that acid and base sites of various strengths occur at the adsorbent surface that exist up to at least 673 K.[18,19] This proves that the surface of hydrotalcite is inhomogeneous. Recently, different models have been proposed to describe the adsorption mechanism of CO_2 by promoted hydrotalcite. Two are Langmuirian based on either one or two sites.[20,21] A kinetic model assuming three different reactions in parallel, all contributing to CO_2 adsorption, was discussed by Ebner et al.[22]

Since there is still no consensus about the adsorption mechanism, we have applied the empirical Freundlich model.

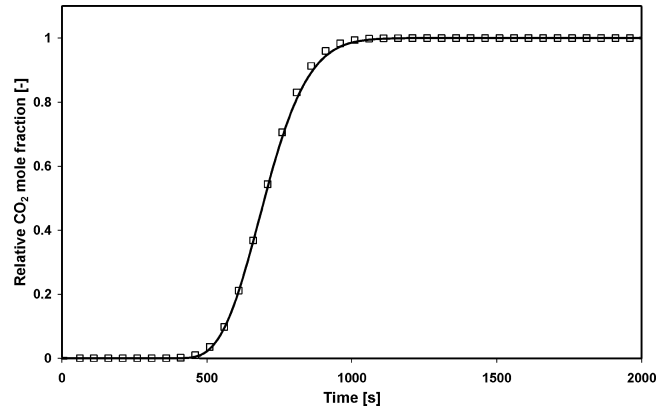

Figure 1. CO_2 mole fraction at the reactor outlet relative to CO_2 mole fraction of the feed gas calculated by the Matlab model (solid line) and from the analytical solution (symbols) for $k_{LDF} = 0.1$ 1/s, $\rho_{b,ads} = 553$ kg/m^3, $T = 673$ K, $H = 6.462 \times 10^{-5}$ mol/kg·Pa, $z = 0.02$ m, $\varepsilon = 0.4$, $v = 0.014$ m/s, and $p_{CO_2} = 1000$ Pa.

Work by our group to disentangle the details of the adsorption mechanism is in progress.

Verification

Verification was performed by comparing the breakthrough curve calculated by the Matlab model with that obtained from an analytical solution for a homogeneous adsorbent bed. The following starting points were used apart from the assumptions mentioned in the section Reactor Model:

• the adsorption isotherm is linear,

• the LDF mass transfer coefficient k_{LDF} is constant,

• pressure p and temperature T are constant throughout the bed,

• axial dispersion does not occur, and

• the concentration of CO_2 is so low that the velocity change is negligible.

For such a system, it can be shown that y_{CO_2} at position z of the bed is given by[22]

$$\frac{y_{CO_2}(z)}{y_{f,CO_2}} = \int_0^\tau \exp(-(\xi + u))I_0(2\sqrt{\xi u})\,du + \exp(-(\xi + \tau))I_0(2\sqrt{\xi\tau}) \tag{10}$$

where I_0 is a zeroth-order modified Bessel function of the first kind,

$$\xi = \frac{k_{LDF}\rho_{b,ads}RTKz}{\varepsilon v} \tag{11}$$

$$\tau = k_{LDF}\left(t - \frac{z}{v}\right) \tag{12}$$

and H (mol/kg·Pa) is defined by

$$q^*_{CO_2} = Hp_{CO_2} \tag{13}$$

Here, $\rho_{b,ads}$ is the bulk density of the adsorbent, v is the interstitial velocity, and ε is the bed porosity. Figure 1 shows the breakthrough curves calculated by both the Matlab model and the analytical solution given by eqs 10−13 using $k_{LDF} = 0.1$ 1/s, $\rho_{b,ads} = 553$ kg/m^3, $T = 673$ K, $H = 6.462 \times 10^{-5}$ mol/kg·Pa, $z = 0.02$ m, $\varepsilon = 0.4$, $v = 0.014$ m/s, and $p_{CO_2} = 1000$ Pa, which are

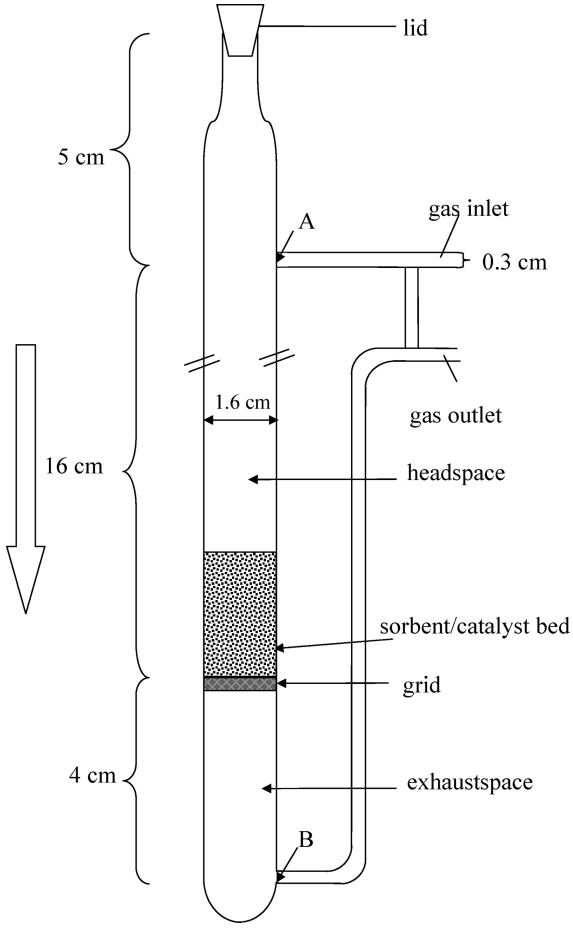

Figure 2. Reactor configuration.

Table 1. Standard Experimental Conditions

	feed step/ adsorption step	regeneration step/ desorption step
flow (mL/min)	30	100
composition	5% CO_2	29% H_2O
	29% H_2O	71% N_2
	66% N_2	
T (K)	673	673
duration (min)	75	75
adsorbent weight (g)	2.2	
particle size (mm)	0.212−0.425	

more or less typical conditions for the experiments reported here. The agreement is excellent.

Experimental Section

The laboratory-scale experiments were carried out in a computer-controlled flow setup, which has been described before.[1] A quartz reactor with an internal diameter of 1.6 cm and a length of ca. 25 cm was placed in a furnace (Figure 2). Here, *headspace* and *exhaustspace* refer to the unfilled reactor parts upstream and downstream of the bed, respectively. The adsorbent sample was placed on a quartz grid, filling only approximately 10% of the total reactor volume. The feed consisted of 5% CO_2 with 29% H_2O in N_2. Regeneration of the adsorbent was performed with 29% H_2O in N_2 in cocurrent direction. Table 1 summarizes the standard experimental conditions that apply unless otherwise specified. Instead of "feed step" and "regeneration step", the terms "adsorption step" and "desorption step" are used respectively. The adsorbent used in all experiments reported here was PURAL MG70 (SASOL),

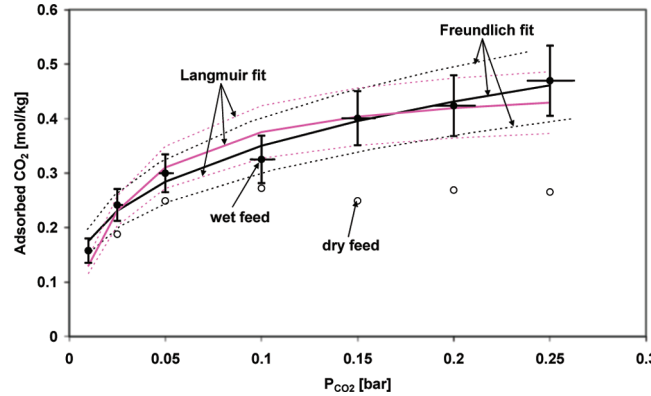

Figure 3. Experimentally determined "adsorption isotherm" of kHTC for dry and wet feed gas (symbols) at 673 K. For the wet isotherm, also the error bars have been indicated. The lines are fits to wet feed gas data (29% H_2O). Solid lines have been fitted to the experimental data, and dashed lines have been determined by the ends of the error bars.

impregnated with 22 wt % K_2CO_3 (Merck). The PURAL MG70 sample as received was calcined for 4 h at 673 K, prior to impregnation. Details of the preparation can be found in a previous paper.[1] For the experiments, 3.0 g fresh adsorbent was used. After the experiments, a final weight of approximately 2.2 g was measured.

The reactor could be bypassed for calibration of the gas composition. Water was removed from the exhaust before analysis was performed. Sampling by a gas chromatograph for CO_2 and N_2 occurred every 75 s. The dry exit gases were also passed into a CO_2 analyzer for CO_2 breakthrough measurements with a higher temporal resolution. A time interval of 15 s was normally used. The results from the gas chromatograph for CO_2 and the CO_2 analyzer after correction were consistent with each other. All experimental data shown here refer to the measured GC data.

The measured CO_2 concentration of the dried gas mixture leaving the reactor plotted versus time elapsed since the start of the feed gas or purge gas supply, yields the breakthrough and desorption profiles for the feed and regeneration steps, respectively. To determine the amount of CO_2 adsorbed and desorbed during respectively the feed and regeneration steps, a blank experiment was performed to correct for instrumental effects. For the blank experiment, a nonadsorbing material (SiC) of the same particle size range and bed volume as the adsorbing samples was used. The experimental conditions were identical to those applied in the experiments using an adsorbing sample. Details of the experimental data analysis can be found in a previous paper.[1]

Adsorption Isotherm

Two sets of experiments were performed, in which the CO_2 concentration of the feed gas was varied between 1 and 25% in successive feed steps. In the first set of experiments, 29% H_2O was present in both the feed and regeneration gases, while in the other set dry feed and regeneration gases were used. The balance was made up with N_2. Other conditions were standard as in Table 1. Figure 3 shows the variation of the adsorbed amount of CO_2 with CO_2 concentration, both for the dry and wet feed gas. In addition, the error bars are shown for the "wet" data. Strictly speaking, it is not *the CO_2 adsorption isotherm of kHTC* for the following reasons:

- the used sample has undergone 20 cycles so that it contains a fraction of sites permanently occupied by strongly bound CO_2,[1]
- other gases (H_2O and N_2) are also present apart from adsorbate gas, and

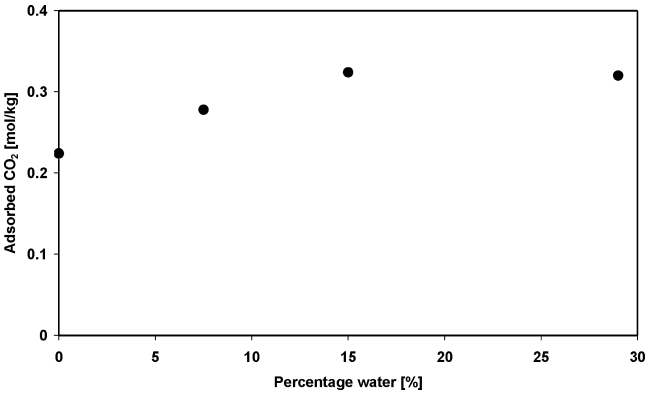

Figure 4. Variation of adsorbed CO_2 with water concentration of the feed gas: (conditions) 673 K, 5% CO_2, balance N_2.

Table 2. Fit Parameters for the Langmuir and Freundlich Isotherms

	Langmuir isotherm		Freundlich isotherm	
	parameter	value	parameter	value
data fit	m (mol/kg)	0.475	k (mol/kg)	0.700
	b (1/Pa)	3.78×10^{-4}	$1/n$ (−)	0.301
upper estimate	m (mol/kg)	0.538	k (mol/kg)	0.807
	b (1/Pa)	3.93×10^{-4}	$1/n$ (−)	0.303
lower estimate	m (mol/kg)	0.412	k (mol/kg)	0.596
	b (1/Pa)	3.67×10^{-4}	$1/n$ (−)	0.297

• the adsorbed amount is not necessarily in equilibrium with the gas-phase CO_2. Nevertheless, we will refer to the data in Figure 3 representing a good approximation of the true adsorption isotherm. From Figure 3, it follows that the presence of water in the feed influences the CO_2 adsorption beneficially. The same phenomenon was found by Ding and Alpay.[24] To investigate this in more detail, an experiment was performed at various H_2O concentrations in the feed gas keeping the CO_2 concentration constant (5%). Other conditions were standard as in Table 1. The results are shown in Figure 4. The H_2O concentration varied between 0 and 29%, the maximum value which can be experimentally obtained. We can see that the adsorbed amount of CO_2 increases more or less linearly between 0 and 15% H_2O by 42%. Between 15 and 29% H_2O, no extra CO_2 is adsorbed. Since water is always present in the SERP feed gas, the wet data were used as input for the code. Fits to the wet data were made, based on both Langmuir and Freundlich isotherms. The error bars were used to make upper and lower estimates of the isotherm. For all fits, the inverse of the error bars served as weight factors for the data points. The parameters of the fits are shown in Table 2. It is not possible to say which isotherm is better. This follows from the analysis of the experiments reported later.

Sorption-Only Experiments and Simulations

The values of the parameters in eqs 3−5 are given in Table 3. More precisely, they apply to the bed part of the reactor. Equations and parameter values for the headspace and exhaustspace are given in the Supporting Information. The parameter values which may change per step (feed gas composition specified by mole fractions y_i, superficial velocity u_f, pressure p_f, and temperature T_f of the feed gas, step duration t_{step}, and wall temperature T_w) are given in Table 4. As pointed out in the paper, a complete cycle of the laboratory-scale experiments consisted of a feed and regeneration step. For the simulations, two steps of short duration were added in which the superficial velocity was gradually changed from its value

Table 3. Parameters of Reactor Bed

quantity	value	quantity	value
ε_b (−)	0.40	μ (kg/m·s)	2.87×10^{-5}
ε_p (−)	0.07	$C_{p,sol}$ (J/kg·K)	850
ε_t (−)	0.44	ΔH_{ads} (J/mol)	−17000
d_p (m)	3.15×10^{-4}	D_m (m^2/s)	7.4×10^{-5}
d_t (m)	0.016	D_p (m^2/s)	1.2×10^{-6}
h (m)	0.020	D_s^o (m^2/s)	1.5×10^{-10}
k_g (W/m·K)	0.025	$\rho_{b,ads}$ (kg/m^3)	553
k_p (W/m·K)	1	$\rho_{p,ads}$ (kg/m^3)	922

Table 4. Conditions of Steps A, B, C, and D

	A	B	C	D
t_{step} (s)	4500	10	4480	10
y_{CO_2}	0.05	0	0	0
y_{H_2O}	0.29	0.29	0.29	0.29
y_{N_2}	0.66	0.71	0.71	0.71
u_f (m/s)	0.0056	0.0056−0.0187	0.0187	0.0187−0.0056
p_f (Pa)	1.01325×10^5	1.01325×10^5	1.01325×10^5	1.01325×10^5
T_f (K)	673	673	673	673
T_w (K)	673	673	673	673

in the feed step to that in the regeneration step, and vice versa (steps B and D, respectively). Without these extra steps, the simulation would not converge. The steps are labeled as A, B, C, and D, where A is the feed step and C the regeneration step, while the velocity changes in steps B and D.

In Figures 5 and 6, the calculated dry CO_2 mole fractions are compared with the data of an experiment using kHTC for the adsorption and desorption steps, respectively. Simulations

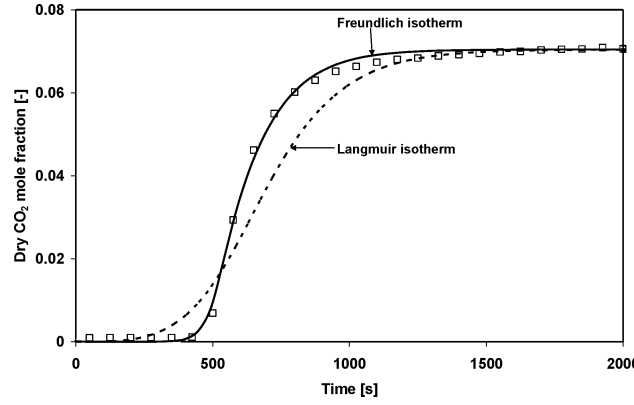

Figure 5. Calculated dry CO_2 mole fraction at the reactor outlet during adsorption using the Freundlich and the Langmuir isotherms, compared with experimental results (symbols): (conditions) 673 K, 5% CO_2, 29% H_2O, 66% N_2, 30 mL/min.

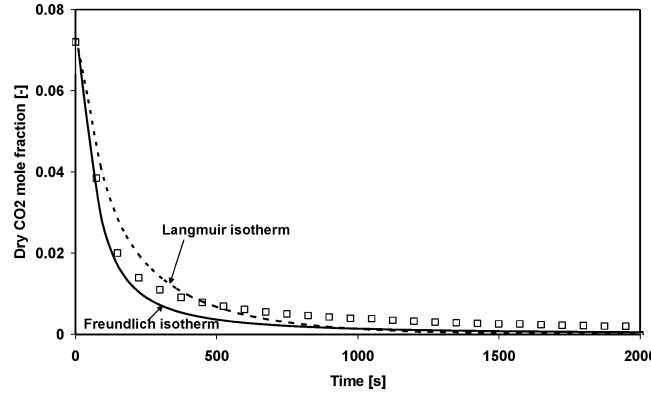

Figure 6. Calculated dry CO_2 mole fraction at the reactor outlet during desorption using the Freundlich and the Langmuir isotherms, compared with experimental results (symbols): (conditions) 673 K, 29% H_2O, 71% N_2, 100 mL/min.

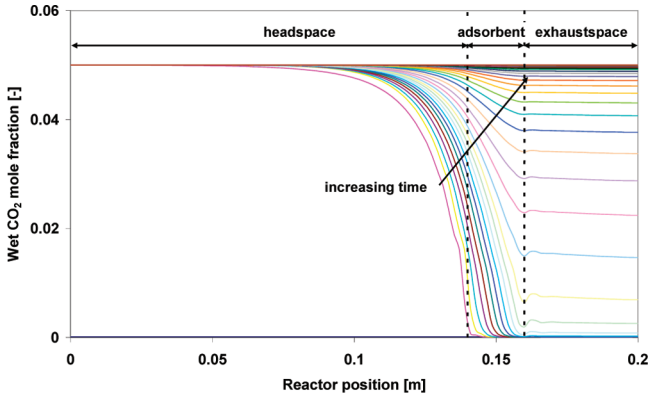

Figure 7. Variation of wet CO_2 mole fraction over the reactor tube during adsorption: (conditions) 673 K, 5% CO_2, 29% H_2O, 66% N_2, 30 mL/min.

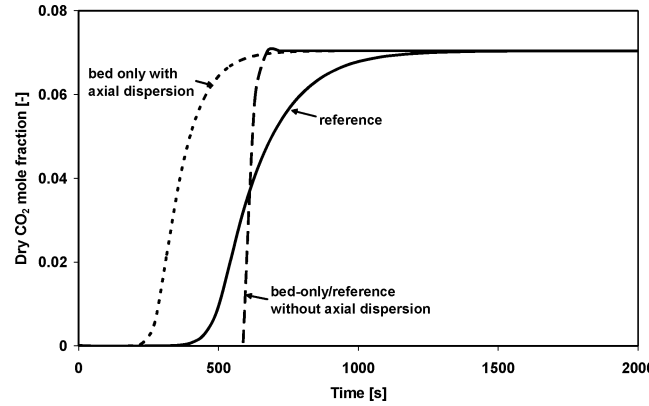

Figure 8. Calculated dry CO_2 mole fraction at reactor outlet during adsorption; bed-only reactor compared with the reference, both with and without axial dispersion: (conditions) 673 K, 5% CO_2, 29% H_2O, 66% N_2, 30 mL/min.

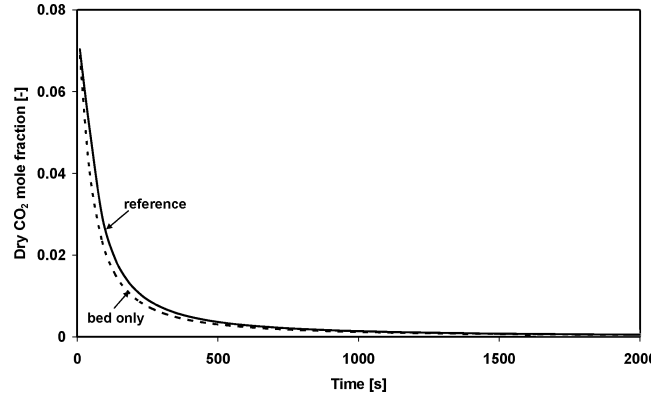

Figure 9. Calculated dry CO_2 mole fraction at reactor outlet during desorption; bed-only reactor compared with the reference, both with axial dispersion: (conditions) 673 K, 29% H_2O, 71% N_2, 100 mL/min.

were performed using both the Langmuir- and Freundlich-based isotherms. Note that the CO_2 mole fraction does not become zero during the desorption step. Instead, a small, non-negligible amount of CO_2 remains present in the purge gas. The Freundlich isotherm yields a better description of the experimental data, especially to the steeply rising part of the breakthrough curve. None of the isotherms, though, is able to simulate the nonzero tail of the desorption curve. The Freundlich-based simulation in Figures 5 and 6 is used as the *reference* and referred to as such throughout this paper. It is necessary to say here that the remaining adsorption and desorption profiles reported here have been checked using both isotherms, and the Freundlich isotherm always gave the better agreement. Therefore, the Freundlich-based simulated results are shown in the rest of the paper.

Figure 7 shows the simulated variation of the wet CO_2 mole fraction in the reactor tube during the adsorption step. The adsorbent bed is positioned between approximately 0.14 and 0.16 m. Upstream and downstream of the adsorbent bed are the headspace and exhaustspace regions, respectively. The wiggles in the calculated profiles, visible at the headspace−bed and bed−exhaustspace boundaries, are numerical artifacts of the simulations and do not have a physical meaning. At the beginning of the adsorption step, CO_2 is strongly adsorbed by the initially empty bed. The resulting strong concentration gradient leads to a large diffusive flux of CO_2 from the headspace region, and consequently, the CO_2 mole fraction shows a large drop from its feed gas value to almost zero. Later on, when the bed gets loaded, the diffusion of CO_2 in the headspace toward the adsorbent bed decreases and the CO_2 mole fraction at the bed inlet shows a steady increase until it has obtained the feed gas value.

Figures 8 and 9 compare a simulation of an imaginary bed-only reactor with the reference. The bed-only reactor contains only the adsorbent bed. The feed gas directly enters the bed without passing the headspace in Figure 2. This has a marked effect on the breakthrough CO_2 profile, which has to do with the applied boundary condition at the reactor inlet ($\partial y_{CO_2}/\partial z = -u_f(y_{f,CO_2} - y_{CO_2})/(\varepsilon_b D_{ax})$ at $z = 0$; see Table 1 of the Supporting Information) and with the fact that the CO_2 concentration starts to change before entering the bed due to diffusion, as discussed above. Neglecting these changes, i.e. assuming that the CO_2 concentration in the feed gas remains unchanged up to the bed inlet, meanwhile maintaining the same inlet boundary condition results in an overestimation of the CO_2 flow entering the bed and, consequently, in a shorter breakthrough time. Normally, this error goes unnoticed since the bed length is usually much larger than the distance over which the concentration change occurs (less than 0.1 m according to Figure 7). If the bed is short, however, as in the laboratory-scale experiments reported here (0.02 m), it will affect the results.

Further, the breakthrough curve of the bed-only case is steeper than that of the reference because of the larger concentration gradient at the bed inlet. When axial dispersion, which is largely determined by molecular diffusion, is excluded from the simulations of both the real reactor and the bed-only reactor, the CO_2 breakthrough curves of both cases coincide since CO_2 diffusion is absent (see Figure 8). It should be noted that the diffusion of CO_2 rapidly decreases with pressure and becomes less important when the feed velocity increases. See for example eq 21 for D_{ij} in the Supporting Information which shows that D_{ij} varies inversely with pressure. Because of the high pressures (between 5 and 20 bar) and feed velocities (at least an order of magnitude larger than in our laboratory-scale experiments) employed in large-scale reactors, diffusive fluxes are much smaller in comparison with convective flows.[8−11]

For the case of an initially empty bed, the breakthrough profiles can be well-described by the model, as shown above, though the desorption profiles cannot. For industrial application of SERP, the bed will be operated cyclically and some CO_2 will remain in the bed after the desorption step. In the following experiments, the bed was not completely desorbed resulting in a partly loaded bed at the start of the feed step. The model can describe the adsorption step well, even though the desorption is incomplete, i.e. when only a fraction of the total CO_2 loading capacity is used. It turns out that this can only be achieved by reducing k_{LDF} during the desorption step. Incomplete desorption

Table 5. Experiments with Variable Desorption Flow and Desorption Duration

variable purge flow		variable desorption duration	
desorption duration: 75 min		desorption flow: 30 mL/min	
desorption flow (mL/min)	prefactor k_{LDF}	duration (min)	prefactor k_{LDF}
100	1	75	0.03
60	0.2	50	0.03
30	0.03	25	0.03
20	0.01	10	0.03
9	0.005		

can be realized experimentally in two ways: by decreasing the purge flow during desorption while keeping the duration of the desorption step unchanged or by decreasing the duration of the desorption step, while keeping the purge flow unchanged. Both ways have been investigated (Table 5). For each condition, five adsorption−desorption cycles were performed. After the third cycle, steady-state was obtained: the CO_2 profiles did not change anymore. Figure 10 shows the experimental and simulated results of an experiment in which the purge flow was reduced. Only the experimental profiles of the fifth cycle for each value of the purge flow are shown. As can be seen from the experimental data, a decrease of the purge flow results in a shorter breakthrough time and a larger CO_2 slip at the beginning of the adsorption step. Good agreement with the data is obtained when the expression of k_{LDF} (eq 21 of the Supporting Information) is multiplied by a prefactor during desorption, the values of which are shown in Table 5.

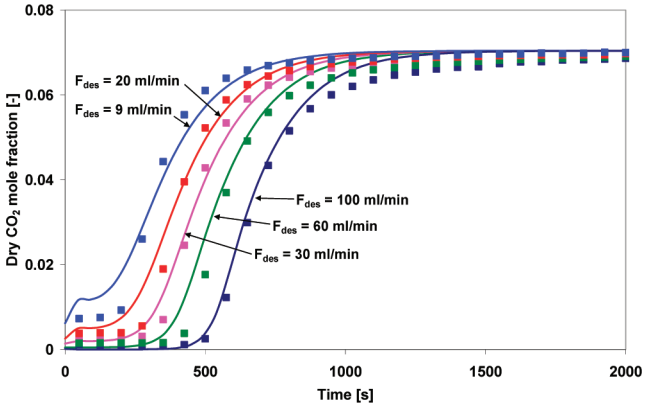

Figure 10. Calculated dry CO_2 mole fraction at reactor outlet during adsorption for various desorption flows as indicated (lines), compared with experimental data (symbols): (conditions) 673 K, 5% CO_2, 29% H_2O, 66% N_2, 30 mL/min.

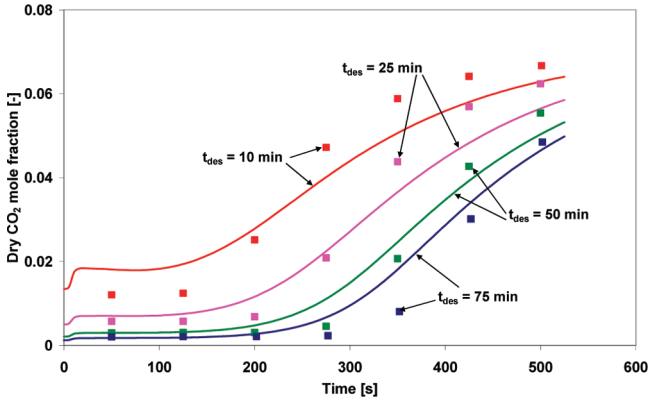

Figure 11. Calculated dry CO_2 mole fraction at reactor outlet during adsorption for various durations of the desorption step as indicated (lines), compared with experimental data (symbols): (conditions) 673 K, 5% CO_2, 29% H_2O, 66% N_2, 30 mL/min.

Table 6. Parameters Values for the Sensitivity Study

varied parameter	lower value	higher value
particle size d_p (m)	2.12×10^{-4}	4.25×10^{-4}
molecular diffusion coefficient D_m (m^2/s)	5.28×10^{-5}	13.6×10^{-5}
ΔH_{ads} (kJ/mol)		115

The smaller the purge flow, the smaller the prefactor. Since mass transport limitations within the particle are already taken into account (see eqs 19 and 20 of the Supporting Information), this cannot explain the prefactor variation with purge flow. Film diffusion, which is not taken into account by the model, may partly account for this. The mass transfer coefficient due to film diffusion k_f varies with flow F according to $k_f \propto F^{0.64}$ for $3 < Re < 2000$.[25] Thus, for a flow decrease from 100 to 9 mL/min, k_f is reduced by a factor 4.7, though the observed decrease of the prefactor amounts to a factor 200. An explanation for this deviation may be found in the unknown details of the desorption mechanism. The Freundlich isotherm model used here is a simplification of the real processes taking place, and it is not based on a physical model. Ebner et al. have shown that three CO_2 sorption processes are taking place in kHTC, each with its own kinetic parameters.[22] A better knowledge of the adsorption and desorption mechanism may help to understand the strong delay of CO_2 release observed during the desorption step in the above experiments.

Figure 11 shows the results of an experiment in which the duration of the desorption step was reduced, the purge flow being the same in all cases. Again, the breakthrough time decreases and the CO_2 slip at the start of adsorption increases when the duration of the desorption step is reduced. Contrary to variable purge flow, the same prefactor could be used for all durations here. This shows that the prefactor depends on the flow, not on the duration of the step.

Sensitivity Analysis

The sensitivity of the CO_2 adsorption and desorption profiles of the reference with respect to the following parameters has been investigated:

- isotherm parameters,
- particle size d_p,
- molecular diffusion coefficient D_m, and
- ΔH_{ads}.

Table 2 shows the values of the isotherm parameters, and Table 6, the values of the other parameters used for the sensitivity study. The values of d_p were determined by the lower and upper limits of the sieve fraction, and those of D_m, by the

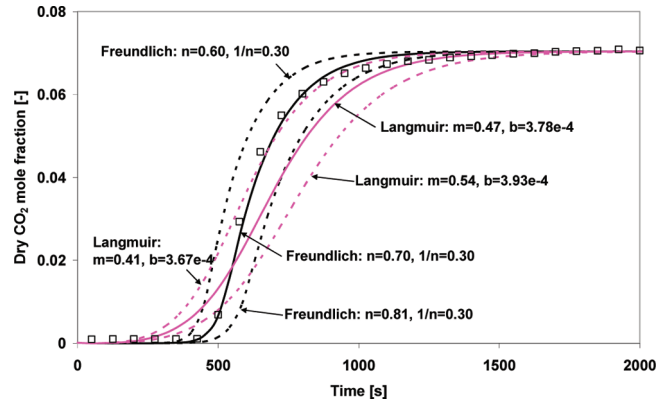

Figure 12. Dry CO_2 mole fraction at reactor outlet during adsorption; sensitivity study results: (conditions) 673 K, 5% CO_2, 29% H_2O, 66% N_2, 30 mL/min.

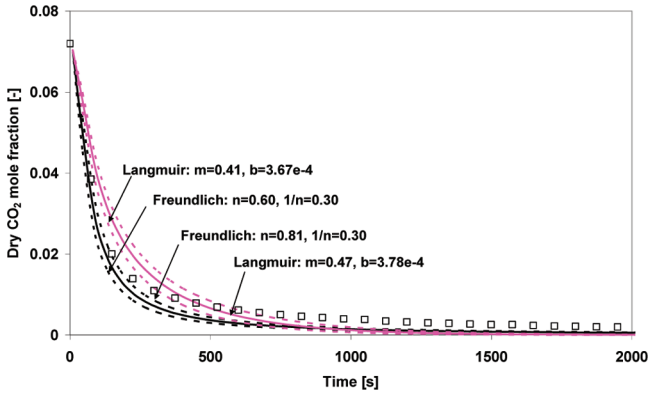

Figure 13. Dry CO_2 mole fraction at reactor outlet during desorption; sensitivity study results: (conditions) 673 K, 29% H_2O, 71% N_2, 100 mL/min.

minimum and maximum values of the calculated diffusion coefficients of pairs of molecules. The values of the varied parameters were applied to both the adsorption and desorption step. Figures 12 and 13 show the adsorption and desorption profiles, respectively, using both the Freundlich and Langmuir isotherms obtained by using the parameter values of Table 2. The effect of the upper and lower estimates on the breakthrough profiles is increasing and decreasing the stoichiometric breakthrough time, respectively, while the slopes of the isotherms remain unchanged. Varying d_p or ΔH_{ads} hardly influences the adsorption and desorption profiles, while decreasing or increasing D_m results in a steeper or less steeper slope of the breakthrough profile, respectively.

Conclusions

A nonisothermal, nonisobaric, and one-dimensional dynamic reactor model has been developed and validated using the results of CO_2 sorption-only laboratory-scale experiments. Here, potassium-promoted hydrotalcite was used as CO_2 adsorbent. The following conclusions can be drawn:

1. The measured CO_2 breakthrough profile can be well-described by the Freundlich isotherm, though not so well by the Langmuir isotherm. Neither isotherm can simulate the desorption profile satisfactorily. Especially the nonvanishing tail of remaining CO_2 in the purge gas turns out to be impossible to simulate.

2. The breakthrough curves calculated by the Matlab model and an analytical solution for the same conditions agree well.

3. The presence of a headspace upstream of the adsorbent bed in the reactor proves to have a significant influence on the breakthrough profile of CO_2 in laboratory-scale due to the occurrence of diffusive fluxes.

4. The model predicts the breakthrough profiles also satisfactorily, when only part of the bed is desorbed, provided that the mass transfer coefficient is changed by a factor during desorption. This adjustment of the mass transfer coefficient reflects the present lack of knowledge of the exact mechanism for desorption of CO_2 from potassium-promoted hydrotalcite.

5. A sensitivity analysis shows that, at the conditions of the laboratory-scale experiments, the rapidly changing parts of the breakthrough and desorption profiles of CO_2 are sensitive to changes of the isotherm parameters and molecular diffusion coefficient, while they are hardly sensitive to changes of the particle size, and the heat of adsorption of CO_2.

Acknowledgment

This research has been carried out by ECN in the CATO-project. CATO (Carbon Capture, Transport and Storage) is the Dutch national research programme on CO_2 Capture and Storage (www.co2-cato.nl). The Dutch government supports CATO with a 50% subsidy from the BSIK programme of the Ministry of Economic Affairs.

Supporting Information Available: Method to solve the set equations including material balance, energy balance, and momentum balance simultaneously; relations for the quantities in the equations and also the parameter values; derivation of the various diffusion coefficients (molecular diffusion coefficient and the coefficient for pore and surface diffusion within the pores of the adsorbent particle), the effect of the adopted model isotherm on the mass transfer coefficient, and the comparison of experimental and simulated results. This material is available free of charge via the Internet at http://pubs.acs.org.

Literature Cited

(1) Reijers, H. Th. J.; Valster-Schiermeier, S. A. E.; Cobden, P. D.; van den Brink, R. W. Hydrotalcite as CO_2 Sorbent for Sorption-Enhanced Steam Reforming of Methane. *Ind. Eng. Chem. Res.* **2006**, *45*, 2522–2530.

(2) Allam, R. J.; Chiang, R.; Hufton, J. R.; Middleton, P.; Weist, E. L.; White, V. Development of the sorption enhanced water gas shift process. In *Carbon Dioxide Capture for Storage in Deep Geologic Formations—Results from the CO_2 Capture Project*; Thomas, D. C., Benson, S. M., Eds.; Elsevier: Oxford, 2005; Chapter 13, Vol. 1.

(3) Cobden, P. D.; van Beurden, P.; Reijers, H. Th. J.; Elzinga, G. D.; Kluiters, S. C. A.; Dijkstra, J. W.; Jansen, D.; van den Brink, R. W. Sorption-enhanced hydrogen production for pre-combustion CO_2 capture: Thermodynamic analysis and experimental results. *Int. J. Greenhouse Gas Control* **2007**, *1*, 170–179.

(4) Waldron, W. F.; Hufton, J. R.; Sircar, S. Production of Hydrogen by Cyclic Sorption Enhanced Reaction Process. *AIChE J.* **2001**, *47*, 1477–1479.

(5) Hufton, J. R.; Mayorga, S.; Sircar, S. Sorption-enhanced reaction process for hydrogen production. *AIChE J.* **1999**, *45*, 248–256.

(6) Ding, Y.; Alpay, E. Equilibria and kinetics of CO_2 adsorption on hydrotalcite adsorbent. *Chem. Eng. Sci.* **2000**, *55*, 3461–3474.

(7) Reijers, H. Th. J.; Boon, J.; Elzinga, G. D.; Cobden, P. D.; van den Brink, R. W. A modeling study of the sorption-enhanced reaction process for CO_2 capture. II. Application to steam-methane reforming. *Ind. Eng. Chem. Res.*, accepted for publication.

(8) Ding, Y.; Alpay, E. Adsorption-enhanced steam-methane-reforming. *Chem. Eng. Sci.* **2000**, *55*, 3929–3940.

(9) Lee, D. K.; Baek, I. H.; Yoon, W. L. Modeling and simulation for the methane steam reforming enhanced by in situ removal utilizing the CaO carbonation for H_2 production. *Chem. Eng. Sci.* **2004**, *59*, 931–942.

(10) Rusten, H. K.; Ochoa-Fernández, E.; Chen, D.; Jakobsen, H. A. Numerical Investigation of Sorption Enhanced Steam Methane Reforming Using Li_2ZrO_3 as CO_2-acceptor. *Ind. Eng. Chem. Res.* **2007**, *46*, 4435–4443.

(11) Xiu, G.; Li, P.; Rodrigues, A. E. Sorption-enhanced reaction process with reactive regeneration. *Chem. Eng. Sci.* **2002**, *57*, 3893–3908.

(12) Sereno, C.; Rodrigues, A. E. Can steady-state momentum equations be used in modelling pressurization of adsorption beds. *Gas Sep. Purif.* **1993**, *7*, 167–173.

(13) Carberry, J. Heterogeneous Catalysis and Catalytic Kinetics. In *Chemical and Catalytic Reaction Engineering*; Courier Dover Publications: Mineola, New York, 2001; Chapter 8.

(14) Rostrup-Nielsen, J. Catalytic steam reforming. In *Catalysis: Science and Technology V*; Andersen, J. R., Boudart, M., Eds.; Springer-Verlag: New York, 1983; Chapter 1.

(15) Xiu, G.; Li, P.; Rodrigues, A. E. Adsorption-enhanced steam-methane reforming with intraparticle-diffusion limitations. *Chem. Eng. Sci.* **2003**, *93*, 83–93.

(16) Ochoa-Fernández, E.; Rusten, H. K.; Jakobsen, H. A.; Rønning, M.; Holmen, A.; Chen, D. Sorption enhanced hydrogen production by steam methane reforming using Li_2ZrO_3 as sorbent: Sorption kinetics and reactor simulation. *Catal. Today* **2005**, *106*, 41–46.

(17) Ruthven, D. M. Thermodynamics of Adsorption. In *Principles of adsorption and adsorption processes*; Wiley: New York, 1984; Chapter 3.

(18) Diez, V. K.; Apesteguia, C. R.; Di Cosimo, J. I. Effect of the chemical composition on the catalytic performance of Mg_yAlO_x catalysts for alcohol elimination reactions. *J. Catal.* **2003**, *215*, 220–233.

(19) Shen, J.Y.; Tu, M.; Hu, C. Structural and surface acid/base properties of hydrotalcite-derived MgAlO oxides calcined at varying temperatures. *J. Solid State Chem.* **1998**, *137*, 295–301.

(20) Lee, K. B.; Verdooren, A.; Caram, H. S.; Sircar, S. Chemisorption of carbon dioxide on potassium-carbonate-promoted hydrotalcite. *J. Colloid Interface Sci.* **2007**, *308*, 30–39.

(21) Oliveira, E. L. G.; Grande, C. A.; Rodrigues, A. E. CO_2 Sorption on hydrotalcite and alkali-modified (K and Cs) hydrotalcites at high temperatures. *Sep. Purif. Technol.* **2008**, *62*, 137–147.

(22) Ebner, A. D.; Reynolds, S. P.; Ritter, J. A. Non-equilibrium kinetic model that describes the reversible adsorption and desorption behavior of CO_2 in a K-promoted hydrotalcite-like compound. *Ind. Eng. Chem. Res.* **2007**, *46*, 1737–1744.

(23) Ruthven, D. M. Dynamics of Adsorption Columns: Single-Transition Systems. In *Principles of adsorption and adsorption processes*; Wiley: New York, 1984; Chapter 8.

(24) Ding, Y.; Alpay, E. Equilibria and kinetics of high temperature CO_2 adsorption on hydrotalcite adorbent. *Chem. Eng. Sci.* **2000**, *55*, 3461–3474.

(25) Ruthven, D. M. Flow through packed beds. In *Principles of adsorption and adsorption processes*; Wiley: New York, 1984; Chapter 7.

Received for review September 1, 2008
Revised manuscript received February 27, 2009
Accepted April 21, 2009

IE801319Q